Earthq Eng & Eng Vib (2024) 23: 241-260 **DOI**: https://10.1007/s11803-024-2235-y

Seismic safety assessment with non-Gaussian random processes for train-bridge coupled systems

Zhao Han[1, 2†], Gao Lei[1, 2‡], Wei Biao[2‡], Tan Jincheng[2§], Guo Peidong[2§], Jiang Lizhong[2‡] and Xiang Ping[2‡]

1. *Key Laboratory of Geomechanics and Embankment Engineering of Ministry of Education, Hohai University, Nanjing 210024, China*
2. *School of Civil Engineering, Central South University, Changsha 410075, China*

Abstract: Extensive high-speed railway (HSR) network resembled the intricate vascular system of the human body, crisscrossing mainlands. Seismic events, known for their unpredictability, pose a significant threat to both trains and bridges, given the HSR's extended operational duration. Therefore, ensuring the running safety of train-bridge coupled (TBC) system, primarily composed of simply supported beam bridges, is paramount. Traditional methods like the Monte Carlo method fall short in analyzing this intricate system efficiently. Instead, efficient algorithm like the new point estimate method combined with moment expansion approximation (NPEM-MEA) is applied to study random responses of numerical simulation TBC systems. Validation of the NPEM-MEA's feasibility is conducted using the Monte Carlo method. Comparative analysis confirms the accuracy and efficiency of the method, with a recommended truncation order of four to six for the NPEM-MEA. Additionally, the influences of seismic magnitude and epicentral distance are discussed based on the random dynamic responses in the TBC system. This methodology not only facilitates seismic safety assessments for TBC systems but also contributes to standard-setting for these systems under earthquake conditions.

Keywords: train-bridge coupled (TBC) system; random vibration; new point estimate method (NPEM); seismic safety assessment; moment expansion approximation (MEA); non-Gaussian distributions

1 Introduction

In 2022, a high-speed railway (HSR) network, appearing like blood vessels do throughout the human body, has already spread across the Chinese mainland. Just as blood vessels should remain unblocked, the safety of this train system should be guaranteed. Bridges comprise a large proportion of the HSR lines, especially simply supported beam bridges (Guo *et al*., 2021). Train-bridge coupled (TBC) vibrations are quite complex under ambient excitations, such as an earthquake occurring when a train is passing across the bridges. An earthquake, as an unpredictable random factor, poses a serious threat to trains and bridges, particularly considering the long operation time of the HSR network (Fig. 1). Therefore, seismic reliability analysis for TBC system

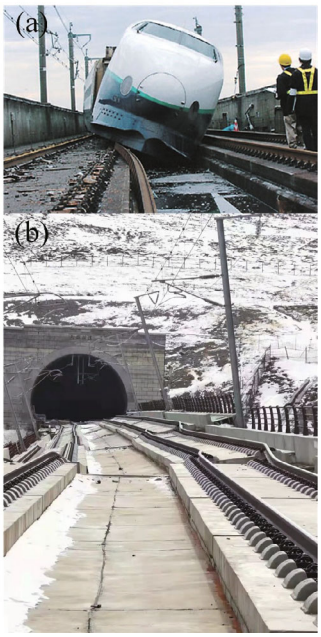

Fig. 1 Earthquake-induced damage in TBC systems: (a) derailment of an HSR train on bridges caused by the Niigata Chuetsu earthquake in Japan (Apostolakis *et al.*, 2007; Ogura, 2006; Zhao *et al*., 2023b); (b) rail bending and track slab cracking resulting from the Qinghai earthquake in China

Correspondence to: Gao Lei, Key Laboratory of Geomechanics and Embankment Engineering of Ministry of Education, Hohai University, Nanjing 210024, China;
Xiang Ping, School of Civil Engineering, Central South University, Changsha 410075, China
Tel.: +86-15802573600
Email: gaoleihhu@hhu.edu.cn (Gao Lei);
pxiang2-c@my.cityu.edu.hk (Xiang Ping)
[†]PhD Candidate; [‡]Professor; [§]Graduate Student

Supported by: National Natural Science Foundation of China under Grant Nos. 11972379 and 42377184, Hunan 100-Talent Plan, Natural Science Foundation of Hunan Province under Grant No. 2022JJ10079, Hunan High-Level Talent Plan under Grant No. 420030004, and Central South University Research Project under Grant Nos. 202045006 (Innovation-Driven Project) and 502390001

Received June 2, 2022; **Accepted** August 28, 2023

has gradually become a burning issue (Zhai *et al*., 2019).

Earthquakes display strong randomness, such as occurrence location, intensity, soil, frequency, etc. (Wang *et al*., 2021b). Therefore, it is inevitable that analyzing some random variables with non-Gaussian processes in seismic design must be carried out. The Monte Carlo method (MCM) is a straightforward and primary method to study random responses of TBC systems (Shao *et al*., 2023). However, it demands a large number of samples for multivariate analysis, a requirement that presently is unacceptable for a complex system. Instead, many efficient algorithms have been applied to study the random analysis of TBC systems, including the pseudo excitation method (Lin *et al*., 1994), the probability density evolution method (Mao *et al*., 2016), the new point estimate method (NPEM) (Jiang *et al*., 2019), deep learning (Li *et al*., 2023; Xiang *et al*., 2023b), and so on.

Different methods are used for various random parameters and problems. Zeng *et al*. (2015a and 2015b) used the pseudo-excitation method to investigate the random vibrations of a high-speed train traversing a slab track on a continuous girder bridge that was subjected to track irregularities and traveling seismic waves. Mao *et al*. (2016) established a random analysis model for a three-dimensional, high-speed train-track-bridge system subjected to random vehicle load, elastic modulus and mass density of a bridge by use of the probability density evolution method. Later, Liu *et al*. applied the point estimate method (PEM) and the NPEM to simulate random rail irregularities and calculate the system dynamic response as subjected to Young's modulus of concrete, damping ratio of concrete, control prestressing stress, and so on (Jiang *et al*., 2019; Liu *et al*., 2020a). They prove that the PEM and NPEM have excellent computational efficiency and applicability to multiple random variables. On balance, the stochastic method is no longer a bottleneck that restricts the development of random vibration analysis for the TBC system in 2022. In contrast, the mathematical mapping models of the system's stochastic characteristics and the safety prediction of system response are still not precise enough.

Random distributions of parameters in random analysis are important features that differs from deterministic dynamic analysis. Previously, the vast majority of random parameters in the TBC system obeyed normal or lognormal distribution, such as initial rail irregularities (Liu *et al*., 2020b), bridge structure parameters (Cho *et al*., 2010; Wang *et al*., 2021a), train parameters (Tan *et al*., 2022), and so on. As a result of the high-precision moment formulas and the convenient triple standard deviation method for determining a confidence interval, Gaussian distribution parameters have been extensively studied and exploited regarding random analysis of TBC systems. However, there exist many critical random parameters that satisfy non-Gaussian distribution in seismic analysis, such as seismic magnitude (SM), epicentral distance (ED), etc. (He *et al*., 2011). Therefore, a compatible and efficient approach is necessary for seismic safety assessment in TBC systems.

In this paper, the NPEM is applied to fast calculate statistical moments of system responses based on the Gaussian integral method (Jiang *et al*., 2020). Furthermore, the moment expansion approximation (MEA) is introduced to obtain the probability density functions (PDFs) of the system responses based on calculated statistical moments. Thus, the statistics can be deduced according to the obtained PDFs. Consequently, the NPEM combined with the MEA (NPEM-MEA) can solve the probabilistic analysis with non-Gaussian processes. More than that, the NPEM-MEA can be helpful for the standard-setting of TBC systems under earthquakes. In addition, the MEA is applicable to the stochastic methods that can calculate the original moment.

The rest of this paper is organized as follows.

Firstly, random variables, the NPEM, and the MEA are illustrated in Section 2.

Secondly, the TBC system shaken by an earthquake is established in Section 3.

Thirdly, some verifications about the NPEM-MEA in the TBC system are conducted in Section 4.

Fourthly, influences of the two different random parameters on the TBC system are studied in Section 5.

Lastly, several conclusions are drawn in Section 6.

2 Methodology

2.1 Random variables

In this seismic analysis, two critical parameters, SM and ED, are considered as random variables of non-Gaussian distributions, and only strong earthquakes (magnitude equal to or greater than six) are adopted. Specifically, the seismic magnitude-frequency statistics satisfy the truncated Gutenberg-Richter distribution (Ji *et al*., 2021; Xu and Gao, 2012; Zhao *et al*., 2022) in this research, which is a complex exponential distribution. Secondly, the ED herein is assumed to be satisfying uniform distribution because the train could be hit by an earthquake at any location.

The PDF of the truncated Gutenberg-Richter model and the relation between the SM and peak ground acceleration (PGA) of the ground motion attenuation model employed in the paper can be formulated as Eqs. (1) and (3), respectively (Pang *et al*., 2020, 2022; Zhao *et al*., 2022).

$$f(m_j) = I_{[m_0, M_u]}(y) \cdot t \exp[-t(m_j - m_0)] / \{1 - \exp[-t(M_u - m_0)]\} \tag{1}$$

with

$$I_{[m_0,\,M_u]}(y)=\begin{cases}0 & \text{if } y\le m_0\\ 1 & \text{if } m_0\le y\le M_u\\ 0 & \text{if } M_u\le y\end{cases} \tag{2}$$

$$\lg a_E = A + Bm_j + C\lg\left(R_{eq}+D\mathrm{e}^{Em_j}\right) \tag{3}$$

where $t=b\ln 10$, $b=0.85$; a_E represents seismic PGA; m_j means the SM; M_u are the lower and upper limit of seismic magnitude, which are six and nine, respectively; R_{eq} denotes the random ED, whose value range is (10 km, 100 km); A, B, C, D and E are all regression coefficients of the elliptical attenuation relationship, which are listed in Table 1. The coefficients of the eastern active region are used in this research.

2.2 New point estimate method

The PEM provides a practical solution for reducing computation costs in stochastic analysis (Zhao and Lu, 2008, 2021). However, the early PEM's computational efficiency is still low due to the complexity of structural response functions. Eventually, the PEM was greatly improved so that the NPEM became one of the mainstream estimation methods, by virtue of introducing the reduced dimension method and an approximation model (Cai *et al*., 2019; Zhao and Lu, 2021) to the response function. Nevertheless, it cannot solve a random analysis with a non-Gaussian process. In this connection, this research employs a method that combines the NPEM and the MEA to fill this gap. The details are presented as follows, and the flow chart of the NPEM-MEA is pictured in Fig. 2.

First, the distributions of random parameters should be determined and then standardized based on the Nataf transformation (Zhao and Ono, 2000). In this research, the random parameters can be expressed as listed below (Lu *et al*., 2017; Zhao *et al*., 2021):

$$X_i = F^{-1}(\Phi(Y_i)) \tag{4}$$

where X_i means the random variable after the Nataf transformation, $\Phi(\bullet)$ means the standard normal cumulative distribution function, $F^{-1}(\bullet)$ means the inverse function of the cumulative distribution function, and Y_i represents the Gauss point of a standard Gaussian distribution.

Second, the number of Gauss point r and a reference point μ_c must be confirmed, and the reduced dimension

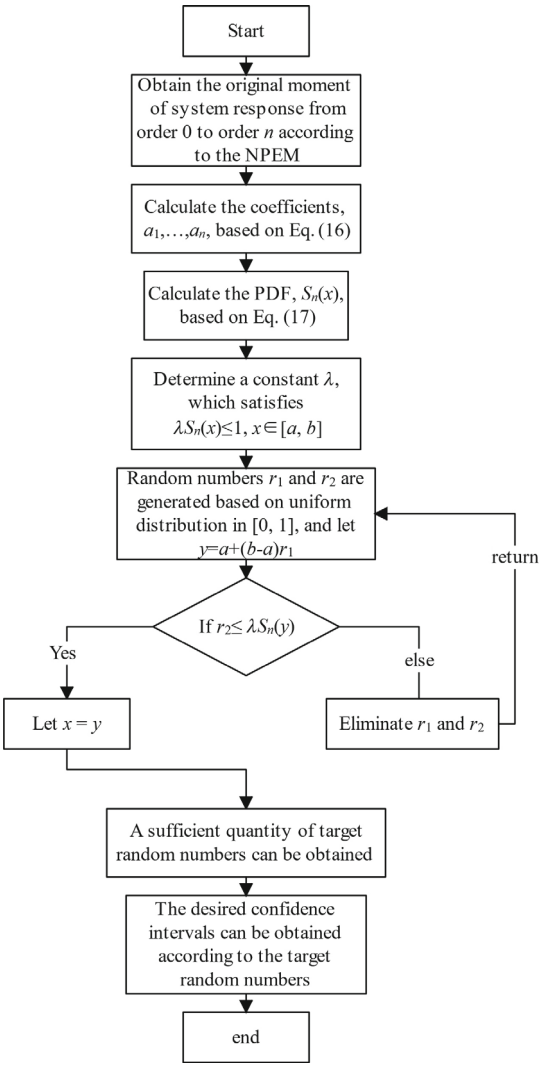

Fig. 2 Flowchart illustrating the NPEM-MEA computational framework

Table 1 Coefficients of the elliptical attenuation relationship of a_E for the Chinese mainland (all data can be referred to in Ref. (Zhao *et al*., 2022))

Region		*A*	*B*	*C*	*D*	*E*
Xinjiang region	Major axis	3.403	0.472	–2.389	1.772	0.424
	Minor axis	2.610	0.463	–2.118	0.825	0.465
Qingzang region	Major axis	3.807	0.411	–2.416	2.647	0.366
	Minor axis	2.457	0.388	–1.854	0.612	0.457
Eastern active region	Major axis	3.533	0.432	–2.315	2.088	0.399
	Minor axis	2.753	0.418	–2.004	0.944	0.447
Moderate seismic region	Major axis	3.706	0.298	–2.079	2.802	0.295
	Minor axis	2.690	0.321	–1.723	1.295	0.331

method and an approximation model are introduced to solve multiple parameters. For explaining the reduced dimension method, the structural response function containing n random variables is assumed as $h(x)$, $\boldsymbol{X}=[x_1,x_2,\cdots,x_n]$, and a dimension-reduction formula can be expressed as follows (Zhao and Lu, 2021):

$$h(X)\cong h^s(X)=\sum_{i=0}^{s}(-1)^i C_{n-s+i-1}^{i}\sum_{k_1<\cdots<k_{s-i}} y_{s-i} \tag{5}$$

where $s<n$,
$y_{s-i}=h\left(c_1,\cdots,c_{k_1-1},x_{k_1},c_{k_1+1},\cdots,c_{k_{s-i}-1},x_{k_{s-i}},c_{k_{s-i}+1},\cdots,c_n\right)$,
$c_1,c_2,\cdots,c_n$ means a set of reference points. Additionally, $s=2$ herein.

Third, each estimate point $\sqrt{2}x_{k,i}$ (subscript k and i represent the ith Gauss point of the kth random parameter, similarly hereinafter) should be substituted into Eq. (4) as Y_i, and then the calculated $X_{k,i}$ ought to be taken into the TBC system as parameters. Next, the structural time-history response $h\left(X_{k,i},t\right)$ can be obtained.

Fourth, the actual time-history response moments (the mean value $\mu(t)$, the qth order central moment $M_{cq}(t)$ and the qth order original moment $M_{oq}(t)$ at each time point can be calculated by substituting the $h\left(X_l,t\right)$ (X_l means a summation of all Gauss points of the lth random variable considering weights, similarly hereinafter) and $h\left(X_l,X_m,t\right)$ into Eq. (6) through Eq. (8), which are (Jiang *et al*., 2019; Zhang *et al*., 2023):

$$\mu(t)\approx\sum_{l<m}E\left[h\left(X_l,X_m,u_c,t\right)\right]-(n-2)\sum_{k=1}^{n}E\left[h\left(X_k,u_c,t\right)\right]+\frac{(n-1)(n-2)}{2}h\left(u_c,t\right) \tag{6}$$

$$M_{cq}(t)\approx\sum_{l<m}E\left[\left(\left[h\left(X_l,X_m,u_c,t\right)\right]-\mu(t)\right)^q\right]-(n-2)\cdot\sum_{k=1}^{n}E\left[\left(h\left(X_k,u_c,t\right)-\mu(t)\right)^q\right]+\frac{(n-1)(n-2)}{2}\left(h\left(u_c,t\right)-\mu(t)\right)^q \tag{7}$$

$$M_{oq}(t)\approx\sum_{l<m}E\left[h\left(X_l,X_m,u_c,t\right)^q\right]-(n-2)\sum_{k=1}^{n}E\left[h\left(X_k,u_c,t\right)^q\right]+\frac{(n-1)(n-2)}{2}h\left(u_c,t\right)^q \tag{8}$$

where n means the number of random parameters, $h\left(u_c,t\right)$ denotes the time-history response when the estimate points are equal to the reference points, and the expectations of some items in Eq. (6) through Eq. (8) are as follows:

$$E\left[\left(\left[h\left(X_k,u_c,t\right)\right]-\mu(t)\right)^q\right]=\sum_{i=1}^{r}\frac{w_{\mathrm{GH},i}}{\sqrt{\pi}}\left(h\left(X_{k,i},u_c,t\right)-\mu(t)\right)^q \tag{9}$$

$$E\left[\left(\left[h\left(X_l,X_m,u_c,t\right)\right]-\mu(t)\right)^q\right]=\sum_{i=1}^{r}\sum_{j=1}^{r}\frac{w_{\mathrm{GH},i}w_{\mathrm{GH},j}}{\pi}\left(h\left(X_{l,i},X_{m,j},u_c,t\right)-\mu(t)\right)^q \tag{10}$$

where r is the number of estimate points (r = 7 is recommended due to the convenience of obtain upper and lower limits of the random variables for the MEA) and $w_{\mathrm{GH},i}$ and $w_{\mathrm{GH},j}$ are the weights of the Gaussian-Hermite estimate point, which can be refer to in specific literature (Jiang *et al*., 2019; Zhao and Lu, 2021).

When considering a single random parameter, such as the kth random variable, Eq. (6) through Eq. (8) can be rewritten as:

$$\mu(t)\approx\sum_{i=1}^{r}E\left[h\left(X_{k,i},u_c,t\right)\right] \tag{11}$$

$$M_{cq}(t)\approx\sum_{i=1}^{r}E\left[\left(h\left(X_{k,i},u_c,t\right)-\mu(t)\right)^q\right] \tag{12}$$

$$M_{oq}(t)\approx\sum_{i=1}^{r}E\left[h\left(X_{k,i},u_c,t\right)^q\right] \tag{13}$$

More details of the NPEM can be referred to in monograph (Zhao and Lu, 2021).

2.3 Moment expansion approximation

Statistics required for safety assessment can be obtained according to the PDFs of system responses (Kolassa, 2006). To obtain the PDFs of such responses, the MEA method can be adopted based on the aforementioned moments obtained according to the NPEM. It should be noted that the MEA method is unsuitable for some special random distributions, such as the Cauchy distribution, but these random distributions rarely appear in the field of TBC.

In the MEA method, the best square approximation function $S_n(x)$ of the target PDF, $f(x)$, exists for a given closed interval [a, b] according to approximation theory (Burden *et al*., 2015), which can be written as follows:

$$\left\|f-S_n\right\|_2^2=\inf\left\|f-S_n\right\|_2^2=\inf\int_a^b\left[f(x)-S_n(x)\right]^2\mathrm{d}x \tag{14}$$

where $\left\|\bullet\right\|_2$ means the Euclidean norm.

Then, according to multivariate extremes theory (Castillo, 2012), the normal function can be obtained as expressed below:

$$\sum_{j=0}^{n}\left(x^k,\,x^j\right)\cdot a_j=\left(f,\,x^k\right),\ \ k=0,\,1,\,\cdots,\,n \tag{15}$$

where (variable 1, variable 2) means the inner product

of variable 1 and variable 2; the polynomial basis of x^k, $x^j \in \mathrm{span}\left\{1, x^1, x^2, \cdots, x^n\right\}$, which are linearly independent of each other, and a_j are the coefficients to be calculated.

Therefore, Eq. (15) can be rewritten in the matrix form:

$$\begin{bmatrix} \int_a^b \mathrm{d}x & \int_a^b x\mathrm{d}x & \cdots & \int_a^b x^n\mathrm{d}x \\ \int_a^b x\mathrm{d}x & \int_a^b x^2\mathrm{d}x & \cdots & \int_a^b x^{n+1}\mathrm{d}x \\ \vdots & \vdots & & \vdots \\ \int_a^b x^n\mathrm{d}x & \int_a^b x^{n+1}\mathrm{d}x & \cdots & \int_a^b x^{n+n}\mathrm{d}x \end{bmatrix} \cdot \begin{bmatrix} a_0 \\ a_1 \\ \vdots \\ a_n \end{bmatrix} = \begin{bmatrix} M_{o0} \\ M_{o1} \\ \vdots \\ M_{oq} \end{bmatrix} \tag{16}$$

where M_{oq} means the n-order original moment (original moments can be gained according to Eq. (8) and Eq. (13) calculated by the NPEM).

After the coefficients a_1, $\cdots$, a_n are calculated, the best square approximation of the PDF can be described as:

$$S_n(x) \approx a_0 x^0 + a_1 x^1 + \cdots + a_n x^n \tag{17}$$

where n denotes the truncation order of moment expansion.

Subsequently, the obtained PDF allows for the generation of random numbers with a high level of precision. This process can be accomplished using the acceptance-rejection method, and it can be organized as follows (Zhao *et al*., 2023c):

(1) A constant should be determined to satisfy $\lambda S_n(x) \leqslant 1$, $x \in [a, b]$.

(2) The random numbers r_1 and r_2 are generated based on the uniform distribution in an interval [0, 1]. Subsequently, let $y = a + (b-a) r_1$.

(3) If $r_2 \leqslant \lambda S_n(y)$, let $x = y$, or else eliminate r_1 and r_2, then repeat step (2).

The cycle repeats itself until sufficient quantities of random numbers, $x_1, x_2, \cdots, x_n$, are generated according to $S_n(x)$. Finally, the desired confidence interval can be obtained based on $x_1, x_2, \cdots, x_n$.

3 TBC simulation system

This section presents a system consisting of an ICE-3 train modeled according to multibody dynamics, ballastless track slab models with three layers of elastic point-support, and a finite element bridge model (Fig. 3(a)). Additionally, the energy variational method is introduced to calculate matrices in the equation of motion (Lou and Zeng, 2005; Xu *et al*., 2020).

3.1 Model of train

An HSR train is a three-dimensional vibration system containing an elastic suspension device. For enhanced numerical efficiency, the car-body, bogies, and wheelsets are assumed to be rigid bodies (Xu *et al*., 2020; Xu and Lu, 2021). Also, the coupler and suspension system of the train are simulated utilizing a three-dimensional linear spring-damper. Each train vehicle has one car-body with six degrees of freedom (DOFs), two bogies with six DOFs each, and four wheelsets with five DOFs apiece (Fig. 3). In addition, details and symbols of the basic motions are listed in Table 2.

The detail of the mass matrix $\boldsymbol{M}_{\mathrm{vv}}$, stiffness matrix $\boldsymbol{K}_{\mathrm{vv}}$ and damping matrix $\boldsymbol{C}_{\mathrm{vv}}$ of the train have the same form as Refs. (Jiang *et al*., 2019; Zhao *et al*., 2023b).

3.2 Model of track slab and bridge

As referenced in Figs. 4(a) and 4(b), multi-span prestressed HSR simply supported box-girder with concrete piers and China railway track system type II slab ballastless tracks are adopted for this research, which is modeled based on the finite element method (Gharad and Sonparote, 2021; Xia *et al*., 2020; Feng *et al*., 2020).

Liu *et al*. (2020a) compared the influence of the Rayleigh damping model and the Caughey damping model and concluded that the Rayleigh damping model is accurate enough to show the dissipation of the system. Therefore, the Rayleigh damping model is adopted for this research, which can be expressed as follows (Zhao *et al*., 2023a):

$$\boldsymbol{C}_{\mathrm{bb}} = \frac{2\omega_i \omega_j \zeta_{\mathrm{b}}}{\omega_i + \omega_j} \boldsymbol{M}_{\mathrm{bb}} + \frac{2\zeta_{\mathrm{b}}}{\omega_i + \omega_j} \boldsymbol{K}_{\mathrm{bb}} \tag{18}$$

where ω_i means the first-order natural circle frequency of the bridge, ω_j means the second-order natural circle frequency of the bridge, and ζ_{b} represents the damping ratio of the bridge.

3.3 Model of wheel-rail contact

The spatial geometric relationship of wheel-rail (WR) contact can be calculated according to the monograph (Zhai, 2020), and the schematic diagram is shown in Fig. 4(c).

The coordinate of the WR contact point in the absolute coordinate system can be deduced as:

Table 2 DOFs of the train

Vehicle components	DOFs					
	Longitudinal	Lateral	Vertical	Roll	Pitch	Yaw
Car-body	x_{c}	y_{c}	z_{c}	θ_{c}	φ_{c}	ψ_{c}
Front bogie	x_{fb}	y_{fb}	z_{fb}	θ_{t1}	φ_{t1}	ψ_{t1}
Rear bogie	x_{rb}	y_{rb}	z_{rb}	θ_{t2}	φ_{t2}	ψ_{t2}
Wheelsets, i=1–4	$x_{\mathrm{w}i}$	$y_{\mathrm{w}i}$	$z_{\mathrm{w}i}$	$\theta_{\mathrm{w}i}$	-	$\psi_{\mathrm{w}i}$

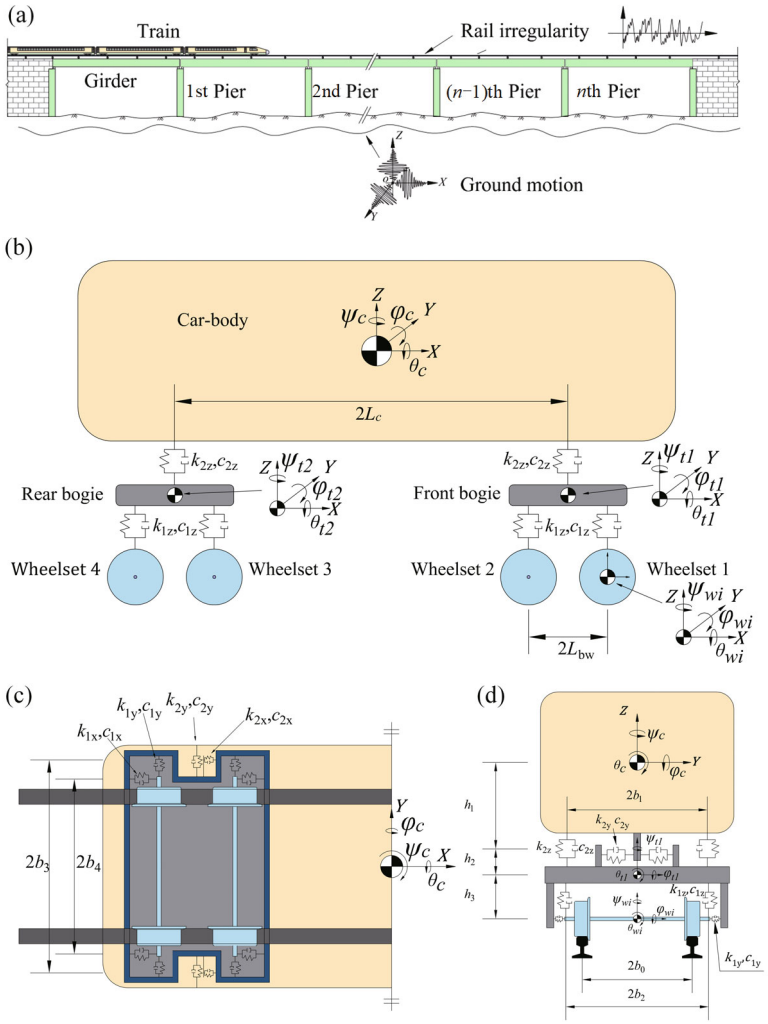

Fig. 3 Schematic representation of the TBC system: (a) overall system, (b) side view, (c) top view and (d) front view of the train vehicle model

$$\begin{cases} x_{C^{\mathrm{R}}} = x_B + l_x R_{\mathrm{w}} \tan\delta_{\mathrm{R}} \\ y_{C^{\mathrm{R}}} = y_B - \dfrac{R_{\mathrm{w}}}{1-l_x^2}\left(l_x^2 l_y \tan\delta_{\mathrm{R}} + l_z\sqrt{1-l_x^2\left(1+\tan^2\delta_{\mathrm{R}}\right)}\right) \\ z_{C^{\mathrm{R}}} = z_B - \dfrac{R_{\mathrm{w}}}{1-l_x^2}\left(l_x^2 l_y \tan\delta_{\mathrm{R}} - l_y\sqrt{1-l_x^2\left(1+\tan^2\delta_{\mathrm{R}}\right)}\right) \end{cases} \tag{19}$$

with

$$\begin{cases} x_B = d_{\mathrm{w}} l_x \\ y_B = d_{\mathrm{w}} l_y + Y_{\mathrm{w}} \\ z_B = d_{\mathrm{w}} l_z \end{cases} \tag{20}$$

$$\begin{cases} l_x = -\sin\varphi_{\mathrm{w}} \cos\psi_{\mathrm{w}} \\ l_y = \cos\varphi_{\mathrm{w}} \cos\psi_{\mathrm{w}} \\ l_z = \sin\varphi_{\mathrm{w}} \end{cases} \tag{21}$$

where

δ_{R} means the contact angle of the right wheel tread;

R_{w} denotes the rolling radius of the wheel;

l_x, l_y, l_z are the direction cosines of the x-axis, y-axis, z-axis, respectively;

x_B, y_B, z_B represent the coordinates of the center of the wheel rolling circle;

d_{w} means the abscissa of the wheel rolling circle in the wheel coordinate.

The WR normal force can be solved by using the nonlinear Hertz elastic contact theory (Guo *et al*., 2023). The WR creep force is formulated according to the Shen-Hedrick-Elkins nonlinear model (Xu and Zhai, 2017). Additional details of the WR contact geometries and forces can be found in the monographs (Kalker, 1990; Zhai, 2020).

3.4 Model of rail irregularity

The influence of primary rail irregularity on dynamic train response has been considered. The rail irregularities in the TBC system are generated according to German low disturbance power spectral density (PSD), based on

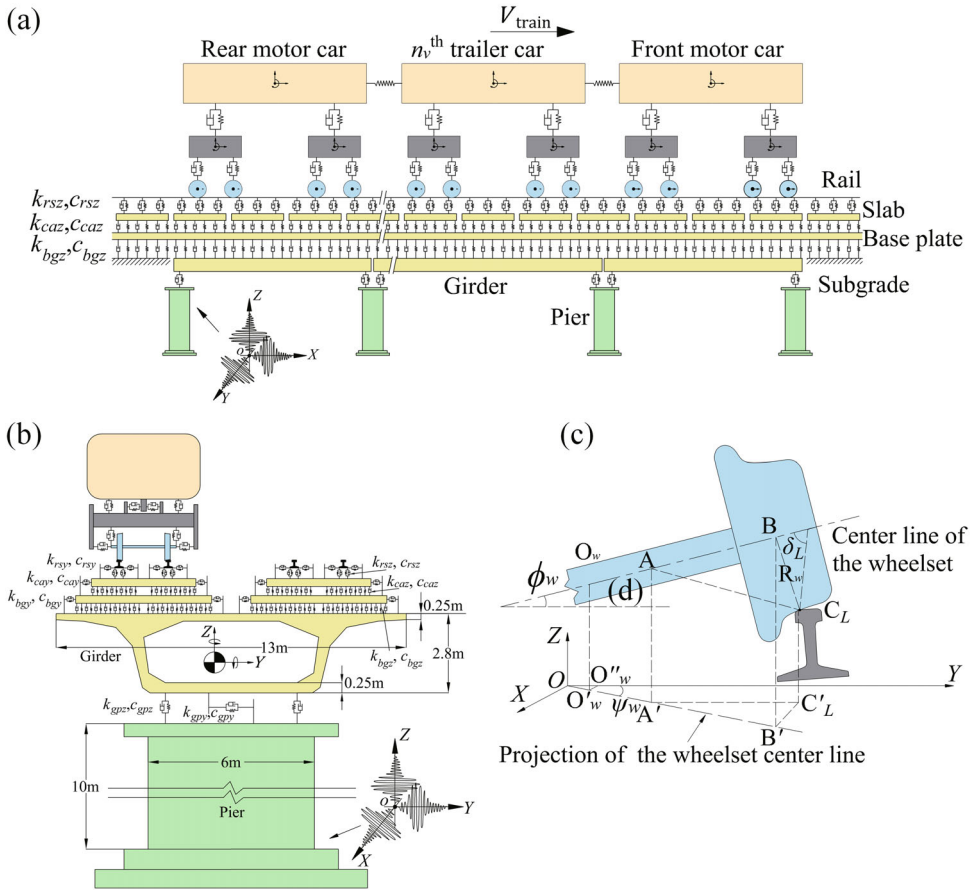

Fig. 4 Diagrams depicting (a) the side view and (b) rear view of the bridge model, along with (c) the WR contact model

the harmonic synthesis method (Chen *et al*., 2013; Jiang *et al*., 2019), which can be expressed as:

$$\begin{cases} S_{\mathrm{v}}(\Omega)=\dfrac{A_{\mathrm{v}}\Omega_{\mathrm{c}}^2}{\left(\Omega^2+\Omega_{\mathrm{r}}^2\right)\left(\Omega^2+\Omega_{\mathrm{c}}^2\right)} \\ S_{\mathrm{a}}(\Omega)=\dfrac{A_{\mathrm{a}}\Omega_{\mathrm{c}}^2}{\left(\Omega^2+\Omega_{\mathrm{r}}^2\right)\left(\Omega^2+\Omega_{\mathrm{c}}^2\right)} \\ S_{\mathrm{c}}(\Omega)=\dfrac{A_{\mathrm{v}}b^{-2}\Omega_{\mathrm{c}}^2\Omega^2}{\left(\Omega^2+\Omega_{\mathrm{r}}^2\right)\left(\Omega^2+\Omega_{\mathrm{c}}^2\right)\left(\Omega^2+\Omega_{\mathrm{s}}^2\right)} \\ S_{\mathrm{g}}(\Omega)=\dfrac{A_{\mathrm{g}}\Omega_{\mathrm{c}}^2\Omega^2}{\left(\Omega^2+\Omega_{\mathrm{r}}^2\right)\left(\Omega^2+\Omega_{\mathrm{c}}^2\right)\left(\Omega^2+\Omega_{\mathrm{s}}^2\right)} \end{cases} \quad (22)$$

where S_{v}, S_{a}, and S_{g} are the irregularity PSD function of vertical rail profile, rail alignment and gauge distance, respectively $\mathrm{m}^2/(\mathrm{rad/m})$;

S_{c} is the PSD function of rail cross-level irregularity $1/(\mathrm{rad/m})$;

A_{v}, A_{a}, and A_{g} represent roughness coefficients;

Ω_{c}, Ω_{r} and Ω_{s} embody truncation frequencies;

and b denotes the half distance between two sides of the rail.

The detailed parameters of the irregularity PSD function are shown in Table 3. The vertical rail profile irregularity of the left rail r^{ZL} and right rail r^{ZR}, and alignment irregularity of left rail r^{YL} and right rail r^{YR} can be referred to in literature (Jiang *et al*., 2019).

3.5 Model of an earthquake

Only a far-field earthquake is adopted for this research, and the Clough-Penzien PSD functions are used to simulate the seismic wave sample, which has a form of (Zeng *et al*., 2015b; Zhang *et al*., 2011):

Table 3 Parameters of German low disturbance PSD of rail irregularity (all data refer to Zhai (2020))

Ω_{c} (rad/m)	Ω_{r} (rad/m)	Ω_{s} (rad/m)	A_{a} ($\mathrm{m^2}$·rad/m)	A_{v} ($\mathrm{m^2}$·rad/m)	A_{g} ($\mathrm{m^2}$·rad/m)
0.8246	0.0206	0.438	2.119×10^{-7}	4.032×10^{-7}	5.32×10^{-7}

$$S_{a_y a_y}(\omega) = \frac{\omega_{gy}^4 + 4\zeta_{gy}^2\omega_{gy}^2\omega^2}{\left(\omega_{gy}^2 - \omega^2\right)^2 + 4\zeta_{gy}^2\omega_{gy}^2\omega^2} \frac{\omega^4}{\left(\omega^2 - \omega_{fy}^2\right)^2 + 4\zeta_{fy}^2\omega_{fy}^2\omega^2} S_{0y} \tag{23}$$

$$S_{a_z a_z}(\omega) = \frac{\omega_{gz}^4 + 4\zeta_{gz}^2\omega_{gz}^2\omega^2}{\left(\omega_{gz}^2 - \omega^2\right)^2 + 4\zeta_{gz}^2\omega_{gz}^2\omega^2} \frac{\omega^4}{\left(\omega^2 - \omega_{fz}^2\right)^2 + 4\zeta_{fz}^2\omega_{fz}^2\omega^2} S_{0z} \tag{24}$$

where ω_{gy} and ω_{gz} denote the predominant frequency of the bridge site;

ζ_{fy} and ζ_{fz} mean the damping ratios of the bridge site;

ζ_{fy}, ζ_{fz}, ω_{fy} and ω_{fz} denote the parameters of the filter;

S_{0y} and S_{0z} represent the spectral intensity factor; and

$\zeta_{gy} = \zeta_{gz}$, $\zeta_{fy} = \zeta_{gy}$, $\zeta_{fz} = \zeta_{gz}$, $\omega_{fy} = 0.1\omega_{gy} - 0.2\omega_{gy}$, $\omega_{fz} = 0.1\omega_{gz} - 0.2\omega_{gz}$ and $S_{0z} = 0.218S_{0y}$.

The other parameters of the PSD functions can be referred to Zhao *et al*. (2022).

Seismic wave has obvious non-stationarity of intensity. Hence, it is described as a product of a stationary filtered wave and a time-varying function in engineering applications (Shinozuka and Sato, 1967), that is:

$$x_{\mathrm{g}}''(t) = D(t)X_{\mathrm{g}}''(t) \tag{25}$$

with

$$D(t) = 12.21 \times (\mathrm{e}^{-0.4t} - \mathrm{e}^{-0.5t}) \tag{26}$$

3.6 Motion equation

In the TBC system, the earthquake loads are treated as external excitations, and the acceleration input mode is adopted. Specifically, it is assumed that the bridge piers are connected to the ground through the supporting nodes. Meanwhile, the dynamic equation of the system is partitioned, as supporting nodes block matrix (supporting nodes) and other structures block matrix (structure nodes) in the absolute coordinate system, which can be expressed as follows (Chopra, 1995; Sun *et al*., 2016; Zhao *et al*., 2023a):

$$\begin{bmatrix} \boldsymbol{M}_{\mathrm{ss}} & \boldsymbol{M}_{\mathrm{sb}} \\ \boldsymbol{M}_{\mathrm{bs}} & \boldsymbol{M}_{\mathrm{bb}} \end{bmatrix} \begin{Bmatrix} \boldsymbol{X}_{\mathrm{s}}'' \\ \boldsymbol{X}_{\mathrm{b}}'' \end{Bmatrix} + \begin{bmatrix} \boldsymbol{C}_{\mathrm{ss}} & \boldsymbol{C}_{\mathrm{sb}} \\ \boldsymbol{C}_{\mathrm{bs}} & \boldsymbol{C}_{\mathrm{bb}} \end{bmatrix} \begin{Bmatrix} \boldsymbol{X}_{\mathrm{s}}' \\ \boldsymbol{X}_{\mathrm{b}}' \end{Bmatrix} + \begin{bmatrix} \boldsymbol{K}_{\mathrm{ss}} & \boldsymbol{K}_{\mathrm{sb}} \\ \boldsymbol{K}_{\mathrm{bs}} & \boldsymbol{K}_{\mathrm{bb}} \end{bmatrix} \begin{Bmatrix} \boldsymbol{X}_{\mathrm{s}} \\ \boldsymbol{X}_{\mathrm{b}} \end{Bmatrix} = \begin{Bmatrix} 0 \\ \boldsymbol{f}_{\mathrm{b}} \end{Bmatrix} \tag{27}$$

where:

$\boldsymbol{X}_{\mathrm{b}}$ means the enforced displacements of the supporting nodes;

$\boldsymbol{X}_{\mathrm{s}}$ represent the displacements of structure nodes;

$\boldsymbol{M}_{\mathrm{ss}}$, $\boldsymbol{C}_{\mathrm{ss}}$ and $\boldsymbol{K}_{\mathrm{ss}}$ are the mass matrix, damping matrix, and stiffness matrix of the structure nodes, respectively;

$\boldsymbol{M}_{\mathrm{bb}}$, $\boldsymbol{C}_{\mathrm{bb}}$ and $\boldsymbol{K}_{\mathrm{bb}}$ are the mass matrix, damping matrix, and stiffness matrix of the supporting nodes, respectively;

$\boldsymbol{M}_{\mathrm{sb}}$, $\boldsymbol{M}_{\mathrm{bs}}$, $\boldsymbol{C}_{\mathrm{sb}}$, $\boldsymbol{C}_{\mathrm{bs}}$, $\boldsymbol{K}_{\mathrm{sb}}$ and $\boldsymbol{K}_{\mathrm{bs}}$ denote the coupling mass matrices, the coupling damping matrices, and the coupling stiffness matrices of the supporting nodes and the structure nodes;

$\boldsymbol{f}_{\mathrm{b}}$ is the force of the supporting nodes subject to the ground.

The first row of Eq. (27) is expanded based on the lumped mass assumption, and it can be calculated that:

$$\boldsymbol{M}_{\mathrm{ss}}\boldsymbol{X}_{\mathrm{s}}'' + \boldsymbol{C}_{\mathrm{ss}}\boldsymbol{X}_{\mathrm{s}}' + \boldsymbol{K}_{\mathrm{ss}}\boldsymbol{X}_{\mathrm{s}} = -\boldsymbol{C}_{\mathrm{sb}}\boldsymbol{X}_{\mathrm{b}}' - \boldsymbol{K}_{\mathrm{sb}}\boldsymbol{X}_{\mathrm{b}} \tag{28}$$

where $\boldsymbol{X}_{\mathrm{s}}$ is decomposed into pseudo-static displacement $\boldsymbol{Y}_{\mathrm{ps}}$ and dynamic displacement $\boldsymbol{Y}_{\mathrm{d}}$, namely:

$$\boldsymbol{X}_{\mathrm{s}} = \boldsymbol{Y}_{\mathrm{ps}} + \boldsymbol{Y}_{\mathrm{d}} \tag{29}$$

The pseudo-static displacement $\boldsymbol{Y}_{\mathrm{ps}}$ satisfies static equilibrium (set dynamic displacements, all velocities and accelerations to zero), hence $\boldsymbol{Y}_{\mathrm{ps}}$ can be deduced as follows (Chopra, 1995):

$$\boldsymbol{Y}_{\mathrm{ps}} = \boldsymbol{R}\boldsymbol{X}_{\mathrm{b}} \tag{30}$$

Naturally, the pseudo-static velocity and acceleration can be obtained based on Eq. (30):

$$\boldsymbol{Y}_{\mathrm{ps}}' = \boldsymbol{R}\boldsymbol{X}_{\mathrm{b}}' \tag{31}$$

$$\boldsymbol{Y}_{\mathrm{ps}}'' = \boldsymbol{R}\boldsymbol{X}_{\mathrm{b}}'' \tag{32}$$

where $\boldsymbol{R} = -\boldsymbol{K}_{\mathrm{ss}}^{-1}\boldsymbol{K}_{\mathrm{sb}}$ represents the influence matrix (Zhao *et al*., 2023).

In particular, the damping force is considered to be proportional to the dynamic velocity $\boldsymbol{Y}_{\mathrm{d}}'$, so Eq. (28) can be transformed into:

$$\boldsymbol{M}_{\mathrm{ss}}\boldsymbol{Y}_{\mathrm{d}}'' + \boldsymbol{C}_{\mathrm{ss}}\boldsymbol{Y}_{\mathrm{d}}' + \boldsymbol{K}_{\mathrm{ss}}\boldsymbol{Y}_{\mathrm{d}} = -\boldsymbol{M}_{\mathrm{ss}}\boldsymbol{Y}_{\mathrm{ps}}'' - \boldsymbol{C}_{\mathrm{sb}}\boldsymbol{X}_{\mathrm{b}} - \boldsymbol{K}_{\mathrm{ss}}\boldsymbol{Y}_{\mathrm{ps}}' - \boldsymbol{K}_{\mathrm{sb}}\boldsymbol{X}_{\mathrm{b}} \tag{33}$$

Afterward, considering Eqs. (31) and (32) ignoring the damping force of the supporting nodes $\boldsymbol{C}_{\mathrm{sb}}\boldsymbol{X}_{\mathrm{b}}'$, Eq. (33) can be recast as:

$$\boldsymbol{M}_{ss}\boldsymbol{Y}_{d}''+\boldsymbol{C}_{ss}\boldsymbol{Y}_{d}'+\boldsymbol{K}_{ss}\boldsymbol{Y}_{d}=-\boldsymbol{M}_{ss}\boldsymbol{R}\boldsymbol{X}_{b}'' \tag{34}$$

In the system, the acceleration of the earthquake is uniformly input for each bridge pier. Thus, the motion equation of the system can be expressed as follows:

$$\boldsymbol{M}_{ss}\boldsymbol{Y}_{d}''+\boldsymbol{C}_{ss}\boldsymbol{Y}_{d}'+\boldsymbol{K}_{ss}\boldsymbol{Y}_{d}=-\boldsymbol{M}_{ss}\boldsymbol{R}\boldsymbol{X}_{g}''(t) \tag{35}$$

where $\boldsymbol{X}_{g}''(t)$ represents the earthquake acceleration of all support nodes in three directions.

4 Verification

In this section, a relatively simple system has been established (Fig. 5(a)), as the low computational efficiency of the MCM. First, an ICE-3 train with two motor vehicles and one trailer vehicle (MTM) is applied. Its main parameters are listed in Table A1. Second, a five-span 32 m prestressed HSR two-way, simply supported box-girder bridge is established based on Section 3.2. The main parameters of the track slab and bridge are listed in Table A2. Third, primary rail irregularities are generated by the use of German low disturbance PSD functions (Section 3.3). Also, a set of three-dimensional artificial seismic waves is adopted (Fig. 5, Secion 3.5). Lastly, the train ran a short distance (about 50 m) before crossing the bridge, and maintained a constant speed (200 km/h) until leaving the bridge. The ground motion is loaded exactly at the instant when the train enters the bridge.

4.1 Verification of random variables

To verify the feasibility and efficiency of each random variable calculated by the NEPM-MEA, a series of calculations are accomplished according to NPEM-7 and MCM-1000 (the numbers mean the number of Gauss points adopted for NPEM and calculation times for MCM, respectively). Thereafter, the comparison of the 3rd car-body response between the MCM-1000 and the NPEM-7 from the 1st to 4th order moment is applied to validate the method. As the topmost unit of the TBC system, the findings are convincing enough to verify the acceleration of the car-body rather than the remaining part of the system.

Figure 6 compares the acceleration time history of the 3rd car-body in the lateral and vertical directions between the NPEM-7 and the MCM-1000, with random

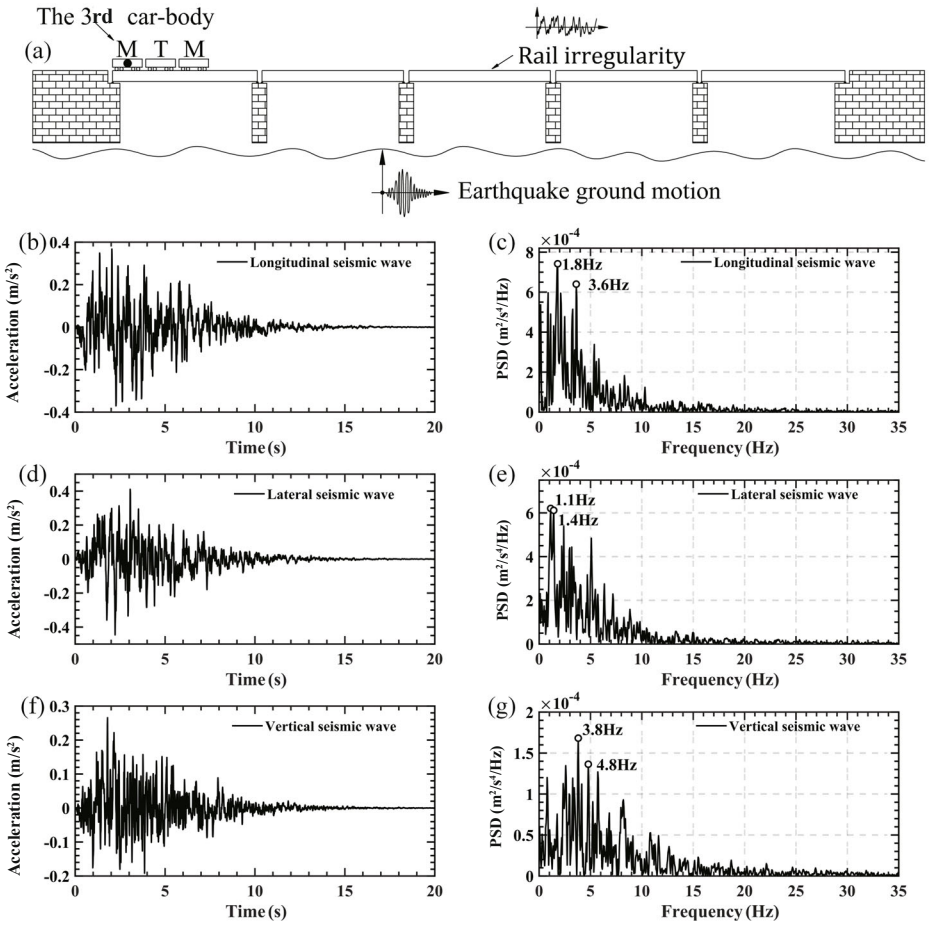

Fig. 5 (a) The schematic diagram of the TBC model, (b, d, f) three-dimensional seismic acceleration time-history curves and (c, e, g) the pertinent PSD curves of the three components

SM. The horizontal axis in each subgraph denotes the distance of the first wheelset passing through the start point. It can be observed that the NPEM-7 curves and the MCM-1000 curves all agree well with one another in both directions and in each subgraph. Furthermore, the simulation results demonstrate that even the 4th central moment, as calculated by the NPEM-7 is still accurate. Regarding calculation efficiency, the NPEM-7 outperforms MCM-1000 by two orders of magnitude in this simulation.

Similarly, Fig. 7 compares the acceleration time histories of the 3rd car-body in the lateral and vertical directions between the NPEM-7 and the MCM-1000, with random ED. Figure 8 compares the acceleration time-histories of the 3rd car-body in the lateral and vertical directions between the NPEM-7 and the MCM-1000, with both random variables. Consistent results in all the subgraphs displayed in Figs. 7 and 8. This consistency confirms that the accuracy of the NPEM-7 is sufficient for different random variables with non-Gaussian distribution characteristics.

4.2 Optimal truncation order of moment expansion

The moments calculated by the NPEM become increasingly inaccurate as the order of moments increases (Jiang *et al*., 2019). Therefore, there is an optimal value for the truncation order of the MEA method. Thereafter, the PDF curves at several randomly selected time points in the 3rd car-body acceleration under MCM-1000 and the NPEM-MEA with different truncation orders are used to find the optimal value.

Different PDF curves of the 3rd car-body acceleration presented in Fig. 9 are generated by the MCM-1000 and the NPEM-MEA, with a truncation order from three to eight in two directions (lateral and vertical) calculated at two points of time (distance = 139 m and distance = 60 m) and with different random variables. The different time points and directions shown in Fig. 9 are chosen randomly for generality. Wherein the PDF curves of MCM-1000 are generated by *ksdensity* function, a built-in function in MATLAB (used version: R2020b), which uses a kernel smoothing function for estimating univariate or bivariate data. More details can be found in MATLAB help files.

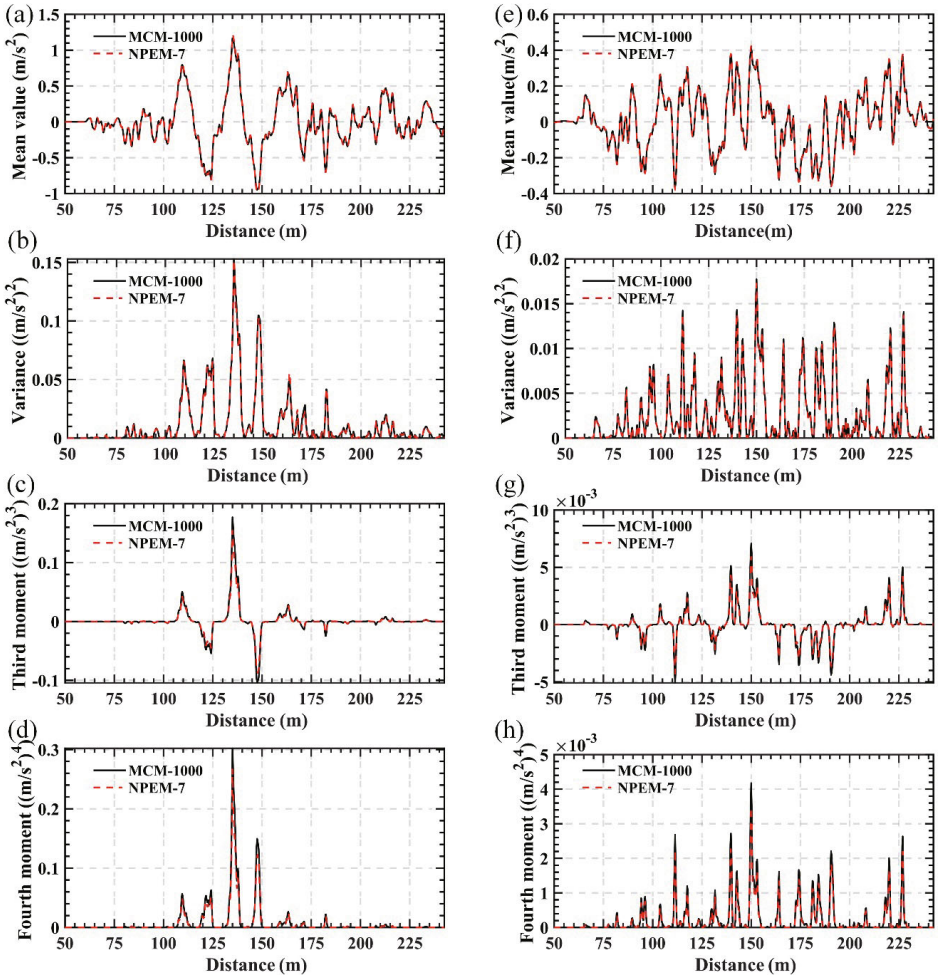

Fig. 6 Comparative analysis of the 3rd car-body's acceleration time-history curves between NPEM-7 and MCM-1000 with random SM: (a) mean value, (b) variance, (c) third moment, and (d) fourth moment in the lateral direction (*y*-direction, similarly hereinafter); (e) mean value, (f) variance, (g) third moment, and (h) fourth moment in the vertical direction (*z*-direction, similarly hereinafter)

This type of probability density estimation method has a significant error at the boundary of the domain, which explains the dropping part (inaccurate part) at the end of the MCM-1000 curves. However, the remainder of the curve is sufficiently accurate (Bowman and Azzalini, 1997). For comparing the PDF curves among different truncation orders, the Euclidean distance approach is introduced, and it is modified as follows to satisfy the demands of this research:

$$D_{\text{Euclidean}} = \sqrt{\frac{1}{n}\sum_{i=1}^{n}\left(y_1(i) - y_2(i)\right)^2} \tag{36}$$

where $y_1(i)$ and $y_2(i)$ are the ith vertical coordinates of the two curves, which have the same abscissa; n means there are n points on the curve with equal abscissa spacing, and n is large enough to ensure accuracy.

Naturally, the smaller the Euclidean distance is, the closer are these two curves, according to Eq. (36). In Fig. 9, the MCM-1000 curves are considered to comprise target curves (in addition to the inaccurate part), and the calculated Euclidean distances are listed in Table 4. By comparison, it can be observed that the NPEM-MEA curves are all close enough to the MCM-1000 curve in each subgraph, but the proximity of these NPEM-MEA curves to the target curves shows a slight difference. Specifically, the NPEM-MEA curves of n = 5 and 6 are closest to the MCM-1000 for Figs. 9(a) and 9(d); the NPEM-MEA curves of n = 3 and 4 correspond to Figs. 9(b) and 9(e); and the NPEM-MEA curves of n = 4 and 5, correspond to Figs. 9(c) and 9(f). Therefore, the optimal truncation order of the NPEM-MEA will change with the random variable, but four to six are accurate enough for the truncation order.

Figure 10 compares acceleration probability curves of the 3rd car-body generated by the MCM-1000 and the NPEM-MEA with a truncation order n = 6 in the vertical direction, with both random variables and at different confidence levels. In addition, the confidence interval curves include the upper and lower curves, and the space between the two curves has a specific probability, which is the confidence level, containing the true value. The confidence interval curves for estimating the response of

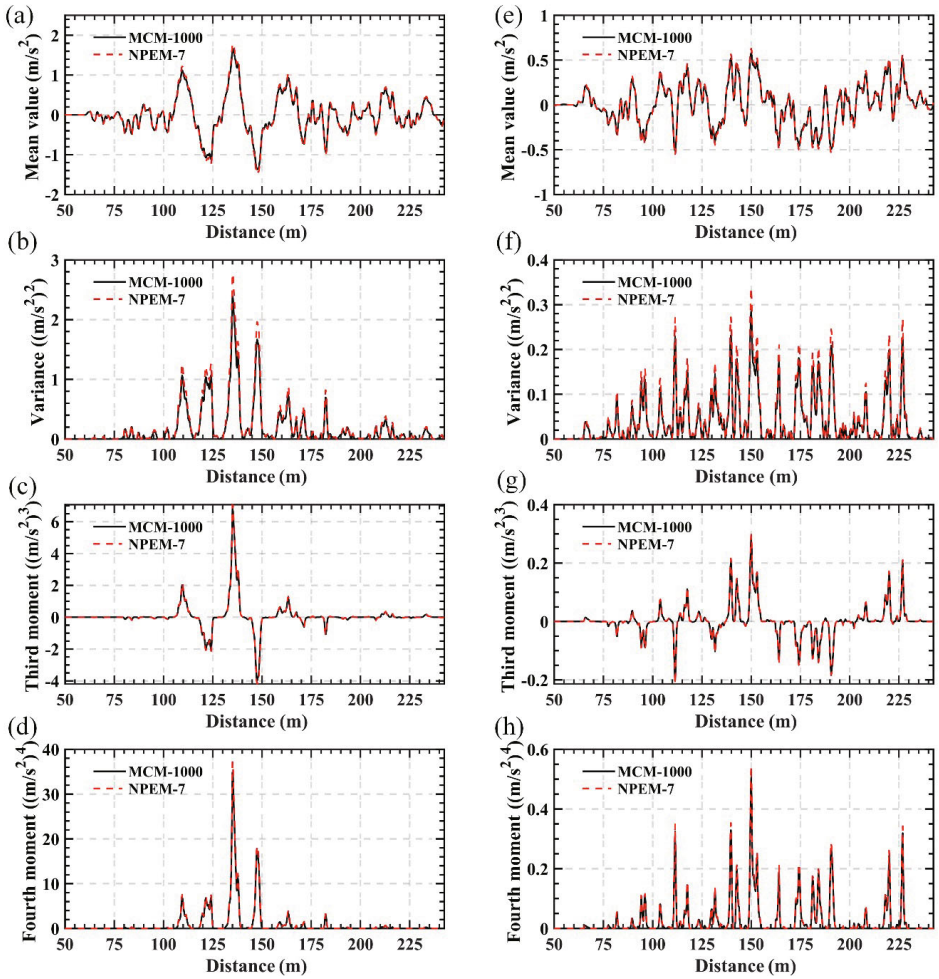

Fig. 7 Comparative analysis of the 3rd car-body's acceleration time-history curves between NPEM-7 and MCM-1000 with random ED: (a) mean value, (b) variance, (c) third moment, and (d) fourth moment in the *y*-direction; (e) mean value, (f) variance, (g) third moment, and (h) fourth moment in the *z*-direction

the TBC system at any designated confidence level can be obtained by means of the NPEM-MEA. However, a confidence level with guiding significance for seismic design results from careful consideration of economics, safety and many other factors, which is still blank at present, will not be studied herein. Therefore, two randomly chosen confidence levels (0.6 and 0.8) are used to validate the confidence interval curves that are generated based on the NPEM-MEA by comparing them with the MCM-1000. According toSecondly, the TBC system shaken by an earthquake is established in Section 3.0, it can be found that the upper and lower curves are almost coincident at both confidence levels. In addition, the computing time of the MEA method is about five minutes (used MATLAB version: R2020b, used CPU: Intel Core i7-10700), and it is negligible compared to the computing time of the NPEM.

5 Safety assessment

A much more complex model can be evaluated within an acceptable computing time according to the NPEM-MEA with multiple non-Gaussian distribution random variables. Therefore, a seven-span, simply supported beam bridge and a train consisting of two motor vehicles and two trailer vehicles (MTTM) are adopted (Fig. 12(a)). Also, the other system's parameters are consistent with Section 4, except that the train's speed is 250 km/h. Thereafter, Figs. 12 and 13 depict the lateral and vertical acceleration time-history curves of the 4th car-body at the three confidence levels, with random SM and ED, respectively, as well as the displacement of the 4th span midpoint.

5.1 Influence of a single random variable

It is impractical to build the HSR railway bridge, which can withstand an earthquake of extreme intensity, considering construction difficulties and attendant economic effects. Since earthquakes cannot be predicted at present, Figs. 12, 13, and 14 can evaluate the response range of the TBC system from the perspective of probability. Additionally, according to vibration criteria for HSR bridges and train vehicles in China (Xia *et al*., 2018; Xiang *et al*., 2023a), it is recommended that a

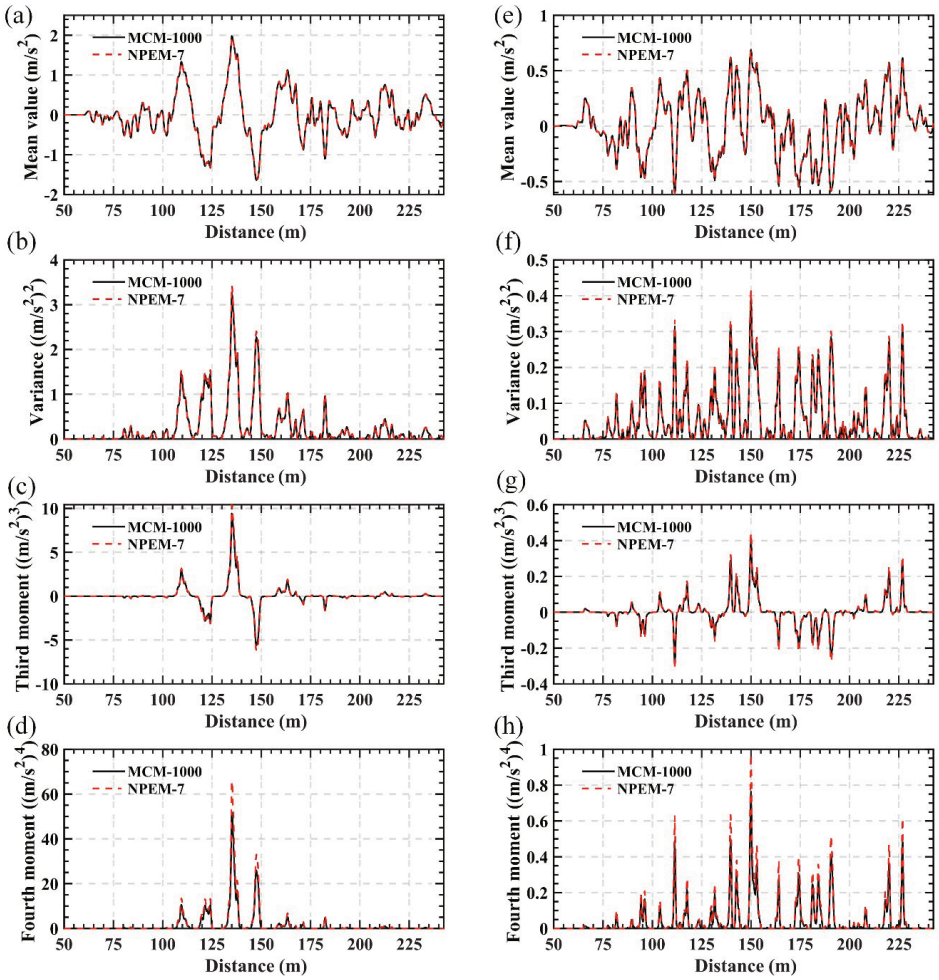

Fig. 8 Comparative analysis of the 3rd car-body's acceleration time-history curves between NPEM-7 and MCM-1000 with both random SM and ED: (a) mean value, (b) variance, (c) third moment, and (d) fourth moment in the *y*-direction; (e) mean value, (f) variance, (g) third moment, and (h) fourth moment in the *z*-direction

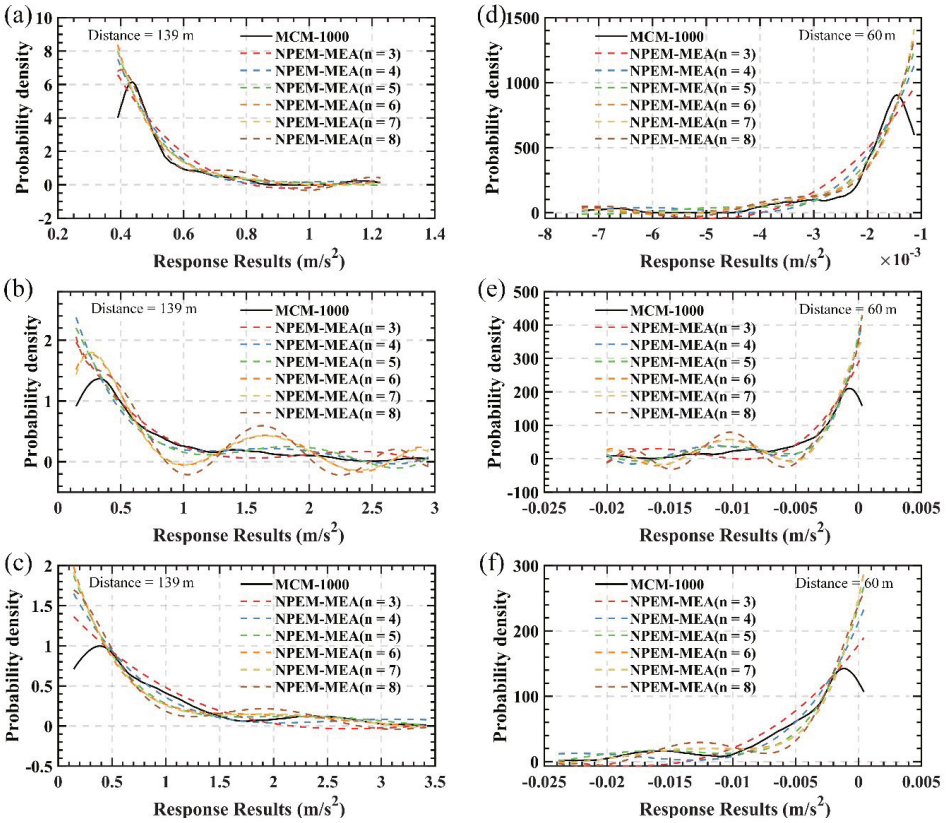

Fig. 9 PDF curves of the 3rd car-body acceleration between the MCM-1000 and the NPEM-MEA with truncation orders from three to eight: (a, b, c) for the time point (distance = 139 m) in the lateral direction (SM, ED, both); and (d, e, f) for the time point (distance = 60 m) in the vertical direction (SM, ED, both)

Table 4 Euclidean distance among different curves

Truncation order	Euclidean distance					
	Fig. 9(a)	Fig. 9(b)	Fig. 9(c)	Fig. 9(d)	Fig. 9(e)	Fig. 9(f)
$n = 3$	0.4719	0.0812	0.0842	76.2949	18.5967	13.6556
$n = 4$	0.3197	0.0700	0.0484	51.4067	15.8192	8.4336
$n = 5$	0.2789	0.0887	0.0554	41.7215	13.6838	8.0005
$n = 6$	0.2754	0.1875	0.0657	42.6831	24.6951	9.5073
$n = 7$	0.2603	0.1861	0.0684	48.2546	25.1419	9.6052
$n = 8$	0.2390	0.2526	0.1084	42.2220	32.6822	15.1627

car-body's lateral and vertical acceleration not to exceed 1.3 m/s^2 and 1.0 m/s^2, respectively. In addition, the lateral displacements of the bridge midpoints should be limited to 3.5 mm. Accordingly, the over-limit area will be considered a dangerous space, and the remaining area will be judged to be safe (Guo *et al.*, 2010). On this basis, three confidence levels are chosen to evaluate the reliability of the TBC system, by which the 0.99 confidence interval curves can be considered the extreme state.

In Fig. 12, it can be seen that for the train, three confidence interval curves exceed its limits in the lateral direction. Meanwhile, the vast majority of the 0.6 area (confidence interval curves enclose the pertinent confidence level areas) is within the safe area in the lateral direction of the bridge. It is found that train running safety is threatened in more than half of the cases when a single random SM is considered. Another finding is that the train and the bridge are much safer in the vertical direction. This particular phenomenon indicates that train running safety is more vulnerable than is the case with the bridge itself.

Conversely, a different situation is displayed in Fig. 13. Three confidence level areas exceed the safe area for both the train and the bridge in the lateral and vertical directions. Therefore, the train and the bridge

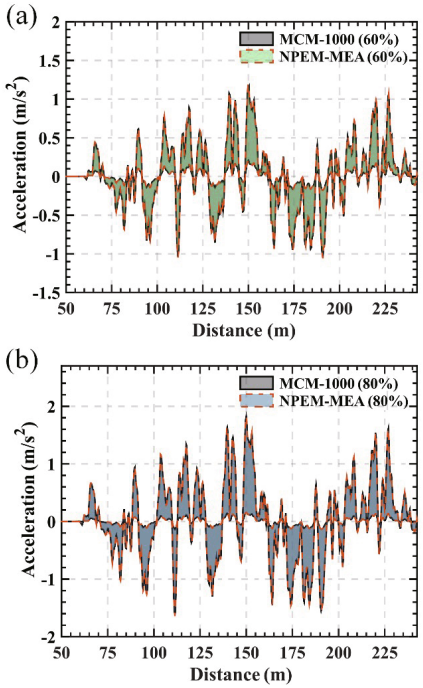

Fig. 10 Acceleration probability curves of the 3rd car-body generated by the MCM-1000 and the NPEM-MEA with truncation order n = 6 in the vertical direction with both random variables for several confidence levels: (a) 0.6, and (b) 0.8

are highly likely to become damaged with a single random ED. Further, the train exhibits a high probability of strong vibration in the vertical direction.

5.2 Influence of both random variables

Figure 14 shows the lateral and vertical acceleration time-history curves of the 4th car-body at the three confidence levels, with both random SM and ED, as well as the displacement of the 4th span midpoint. Subsequently, the standard deviation (Std.D) time-history curves of the train and bridge responses with each random variable are depicted in Fig. 15.

Figure 14 shows that all three confidence level areas seriously exceed the limits for the train and the bridge in both directions. These results reveal a much more dangerous set of circumstances compared to the simulation results with a single random variable, as shown in Figs. 12 and 13. Consequently, an earthquake as a multivariate control system demonstrates a character of high randomness. With regard to seismic reliability analysis, it is necessary to simultaneously consider the randomness of multiple vital parameters. According to Fig. 15, the uncertainty in the dynamic response of the TBC system under the effects of an earthquake can

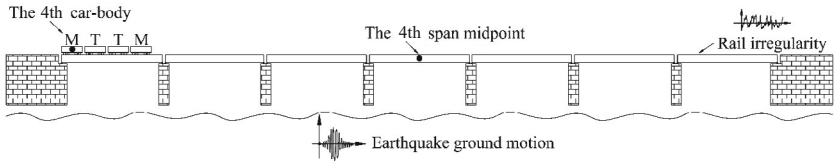

Fig. 11 Schematic diagram of the TBC model

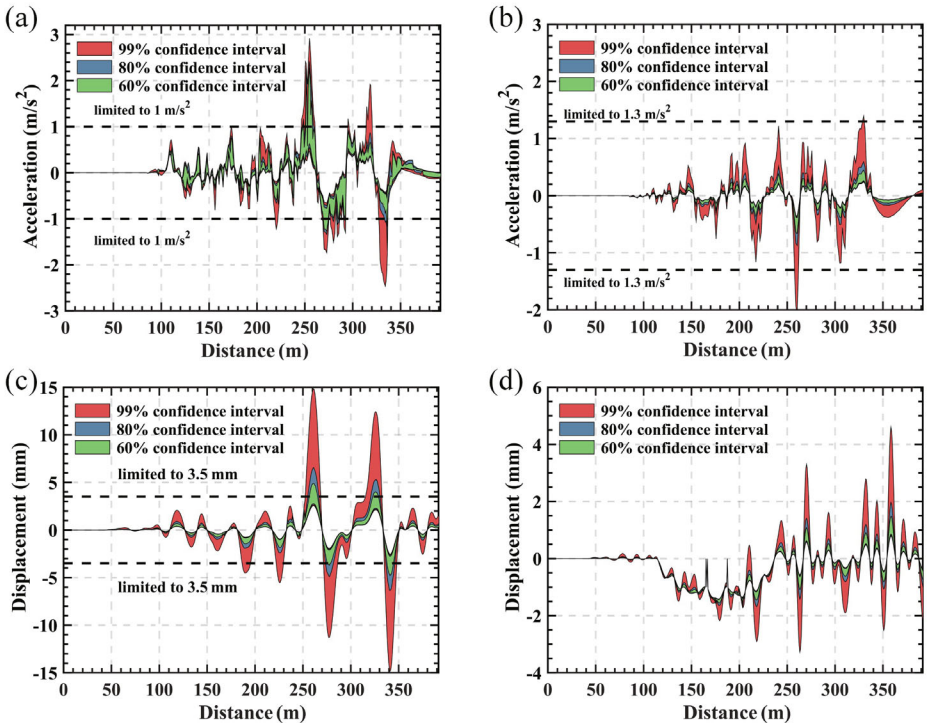

Fig. 12 Train and bridge response safety assessment curves under seismic excitations with the random SM: 4th motor car-body in the (a) y and (b) z directions; 4th span midpoint in the (c) y and (d) z directions

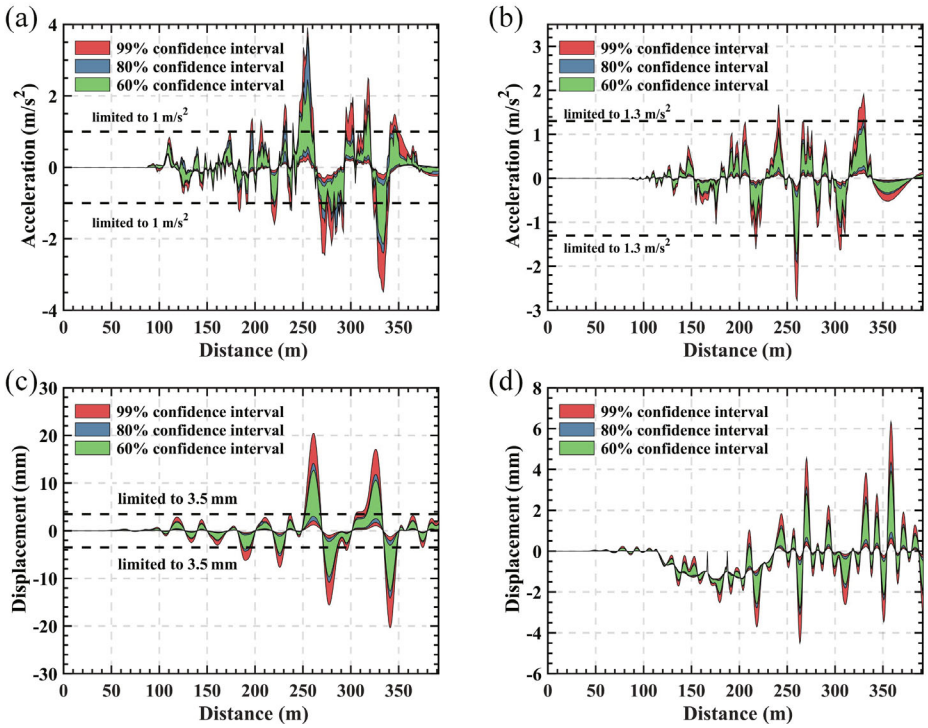

Fig. 13 Train and bridge response safety assessment curves under seismic excitations with the random ED: 4th motor car-body in the (a) *y* and (b) *z* directions; 4th span midpoint in the (c) *y* and (d) *z* directions

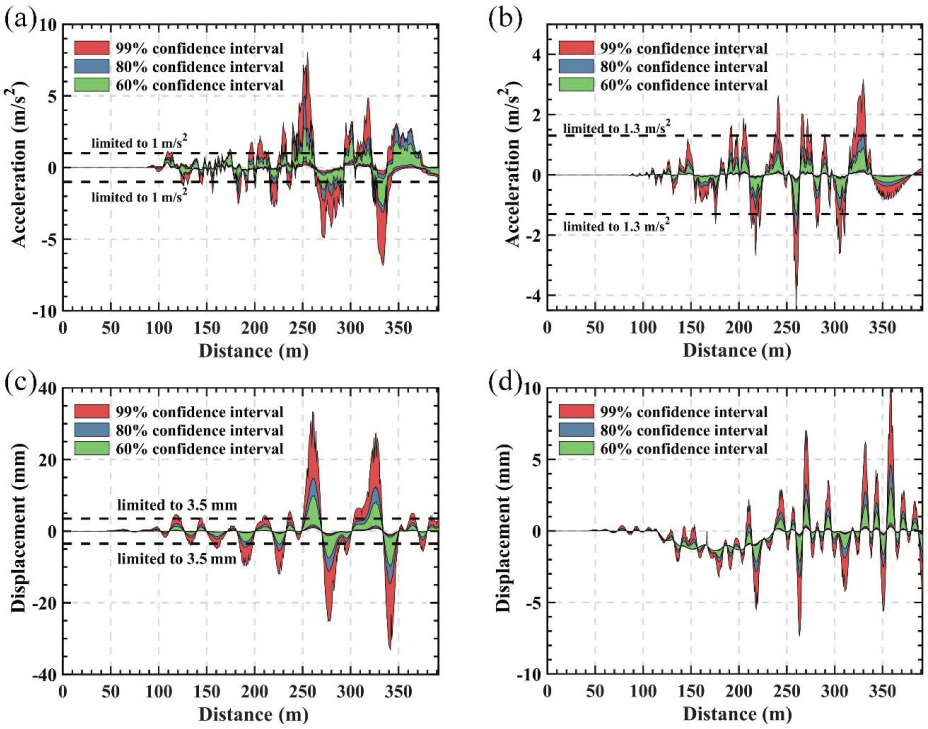

Fig. 14 Train and bridge response safety assessment curves under seismic excitations with both the random SM and ED: 4th motor car-body in the (a) *y* and (b) *z* directions; 4th span midpoint in the (c) *y* and (d) *z* directions

be divided and allocated to different random variables. It can clearly be observed that the Std.D time-history curves of ED are consistently above the curves of SM for the train and the bridge in both directions at any time point when the train is passing across the bridge. There is no doubt that the ED has greater influence than the SM on the response of the train and the bridge.

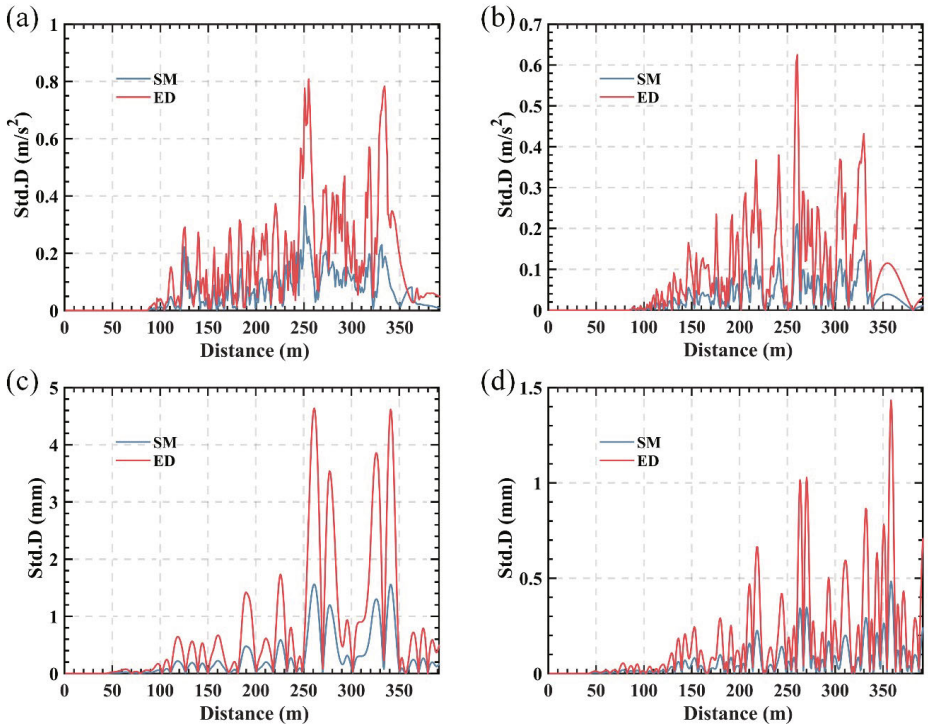

Fig. 15 Std.D time-history curves of the train and bridge response with both the random SM and ED: 4th motor car-body acceleration in the (a) *y* and (b) *z* directions; 4th span midpoint in the (c) *y* and (d) *z* directions

6 Conclusions

This research investigated a seismic safety assessment in an established three-dimensional TBC system with non-Gaussian distribution parameters based on the NPEM-MEA. The NEPM-MEA is verified by comparing it with the simulation results taken from the MCM. A safety assessment of the train and bridge under both random variables is discussed. The main conclusions of the study are as follows:

(1) The NPEM-MEA demonstrates a high degree of accuracy in the seismic safety assessment of the TBC system with non-Gaussian distribution variables, verified by comparing it with the MCM results. In terms of calculation efficiency, the NPEM-7 is two orders of magnitude higher than the MCM-1000.

(2) The recommended truncation order of the NPEM-MEA is 5 or 6 for the random SM, 3 or 4 for the random ED, and 4 or 5 for both SM and ED. The optimal truncation order of the moment expansion will change with different stochastic methods and random distributions of parameters. In addition, four to six will be sufficiently accurate for the truncation order of the NPEM-MEA.

(3) Train running safety is more vulnerable than for the bridge in the lateral direction, and train running safety is threatened in more than half of the cases when considering a single random SM. However, both the train and the bridge are much safer in the vertical direction.

(4) The train and the bridge have a high probability of being damaged, considering random ED. Additionally, the train shows a high probability of strong vibration in the vertical direction, which would seriously affect train running safety. The randomness of ED has a greater influence than that of SM on the response of the train and the bridge in both directions at any time point when the train is passing across the bridge.

(5) From the perspective of probability and the limit state, the responses of the train and the bridge with random SM and ED are significantly higher than those having a single random variable. This highlights the importance of considering the randomness of multiple parameters simultaneously in seismic safety assessment.

References

Apostolakis G, Qu B, Ecemis N and Dogruel S (2007), "Field Reconnaissance of the 2007 Niigata-Chuetsu Oki Earthquake," *Earthquake Engineering and Engineering Vibration*, **6**(4): 317–330. https://doi.org/10.1007/s11803-007-0783-6

Bowman AW and Azzalini A (1997), *Applied Smoothing Techniques for Data Analysis: the Kernel Approach with S-Plus illustrations*, OUP Oxford, UK.

Burden RL, Faires JD and Burden AM (2015), *Numerical Analysis*, Cengage Learning, USA.

Cai CH, Lu ZH, Xu J and Zhao YG (2019), "Efficient Algorithm for Evaluation of Statistical Moments of

Performance Functions," *Journal of Engineering Mechanics*, **145**(1): 06018007. https://doi.org/10.1061/(ASCE)EM.1943-7889.0001551

Castillo E (2012), *Extreme Value Theory in Engineering*, Elsevier, Netherlands.

Chen JB, Sun WL, Li J and Xu J (2013), "Stochastic Harmonic Function Representation of Stochastic Processes," *Journal of Applied Mechanics-Transactions of the ASME*, **80**(1): 011001. https://doi.org/10.1115/1.4006936

Cho T, Song MK and Lee DH (2010), "Reliability Analysis for the Uncertainties in Vehicle and High-Speed Railway Bridge System Based on an Improved Response Surface Method for Nonlinear Limit States," *Nonlinear Dynamics*, **59**(1-2): 1–17. https://doi.org/10.1007/s11071-009-9521-0

Chopra AK (1995), *Dynamics of Structures: Theory and Applications to Earthquake Engineering*, Prentice Hall, USA.

Feng YL, Jiang LZ and Zhou WB (2020), "Dynamic Response of a Three-Beam System with Intermediate Elastic Connections Under a Moving Load/Mass-Spring," *Earthquake Engineering and Engineering Vibration*, **19**(2): 377–395. https://doi.org/10.1007/s11803-020-0568-8

Gharad AM and Sonparote RS (2021), "Evaluation of Vertical Impact Factor Coefficients for Continuous and Integral Railway Bridges Under High-Speed Moving Loads," *Earthquake Engineering and Engineering Vibration*, **20**(2): 495–504. https://doi.org/10.1007/s11803-021-2034-7

Guo P, Zhao H, Xiang P, Liu X, Tan J and Jiang L (2023), "Probabilistic Analysis of High-Speed Train Safety on Bridges Under Stochastic Near-Fault Pulse-Type Ground Motions," *Probabilistic Engineering Mechanics*, **74**: 103527. https://doi.org/10.1016/j.probengmech.2023.103527

Guo W, Wang Y, Liu HY, Long Y, Jiang LZ and Yu ZW (2021), "Running Safety Assessment of Trains on Bridges Under Earthquakes Based on Spectral Intensity Theory," *International Journal of Structural Stability and Dynamics*, **21**(14): 2140008. https://doi.org/10.1142/S0219455421400083

Guo W, Xia H and Xu Y (2010), "Running Safety Analysis of a Train on the Tsing Ma Bridge Under Turbulent Winds," *Earthquake Engineering and Engineering Vibration*, **9**(3): 307–318. https://doi.org/10.1007/s11803-010-0015-3

He XW, Kawatani M, Hayashikawa T and Matsumoto T (2011), "Numerical Analysis on Seismic Response of Shinkansen Bridge-Train Interaction System Under Moderate Earthquakes," *Earthquake Engineering and Engineering Vibration*, **10**(1): 85–97. https://doi.org/10.1007/s11803-011-0049-1

Ji K, Wen RZ, Ren YF, Wang WY and Chen LS (2021), "Disaggregation of Probabilistic Seismic Hazard and Construction of Conditional Spectrum for China," *Bulletin of Earthquake Engineering*, **19**: 5769–5789. https://doi.org/10.1007/s10518-021-01200-2

Jiang LZ, Liu X, Xiang P and Zhou WB (2019), "Train-Bridge System Dynamics Analysis with Uncertain Parameters Based on New Point Estimate Method," *Engineering Structures*, **199**: 109454. https://doi.org/10.1016/j.engstruct.2019.109454

Jiang LZ, Liu X, Zhou T, Xiang P, Chen YJ, Feng YL, Lai ZP and Cao SS (2020), "Application of KLE-PEM for Random Dynamic Analysis of Nonlinear Train-Track-Bridge System," *Shock and Vibration*, **2020**: 8886737. https://doi.org/10.1155/2020/8886737

Kalker JJ (1990), *Three-Dimensional Elastic Bodies in Rolling Contact*, Springer, Netherlands. https://doi.org/10.1007/978-94-015-7889-9

Kolassa JE (2006), *Series Approximation Methods in Statistics*, Springer Science & Business Media, Netherlands.

Li HL, Wang TY and Wu G (2023), "Probabilistic Safety Analysis of Coupled Train-Bridge System Using Deep Learning Based Surrogate Model," *Structure and Infrastructure Engineering*, **19**(8): 1138–1157. https://doi.org/10.1080/15732479.2021.2010104

Lin J, Zhang W and Williams FW (1994), "Pseudo-Excitation Algorithm for Nonstationary Random Seismic Responses," *Engineering Structures*, **16**(4): 270–276. https://doi.org/10.1016/0141-0296(94)90067-1

Liu X, Jiang LZ, Lai ZP, Xiang P and Chen YJ (2020a), "Sensitivity and Dynamic Analysis of Train-Bridge Coupled System with Multiple Random Factors," *Engineering Structures*, **221**(15): 111083. https://doi.org/10.1016/j.engstruct.2020.111083

Liu X, Xiang P, Jiang LZ, Lai ZP, Zhou T and Chen YJ (2020b), "Stochastic Analysis of Train-Bridge System Using the Karhunen-Loeve Expansion and the Point Estimate Method," *International Journal of Structural Stability and Dynamics*, **20**(2): 2050025. https://doi.org/10.1142/S021945542050025x

Lou P and Zeng QY (2005), "Formulation of Equations of Motion of Finite Element Form for Vehicle-Track-Bridge Interaction System with Two Types of Vehicle Model," *International Journal for Numerical Methods in Engineering*, **62**(3): 435–474. https://doi.org/10.1002/nme.1207

Lu ZH, Cai CH and Zhao YG (2017), "Structural Reliability Analysis Including Correlated Random Variables Based on Third-Moment Transformation," *Journal of Structural Engineering*, **143**(8): 04017067. https://doi.org/10.1061/(ASCE)st.1943-541x.0001801

Mao JF, Yu ZW, Xiao YJ, Jin C and Bai Y (2016), "Random Dynamic Analysis of a Train-Bridge Coupled System Involving Random System Parameters Based on Probability Density Evolution Method," *Probabilistic*

Engineering Mechanics, **46**: 48–61. https://doi.org/10.1016/j.probengmech.2016.08.003

Ogura M (2006), "The Niigata Chuetsu Earthquake: Railway Response and Reconstruction," *Japan Railway & Transport Review*, **43–44**: 46–63.

Pang YT, Cai L and Zhong J (2020), "Seismic Performance Evaluation of Fiber-Reinforced Concrete Bridges Under Near-Fault and Far-Field Ground Motions," *Structures*, **28**: 1366–1383. https://doi.org/10.1016/j.istruc.2020.09.049

Pang YT, Wei K, He HF and Wang WX (2022), "Assessment of Lifetime Seismic Resilience of a Long-Span Cable-Stayed Bridge Exposed to Structural Corrosion," *Soil Dynamics and Earthquake Engineering*, **157**: 107275. https://doi.org/10.1016/j.soildyn.2022.107275

Shao ZJ, Li XM and Xiang P (2023), "A New Computational Scheme for Structural Static Stochastic Analysis Based on Karhunen–Loève Expansion and Modified Perturbation Stochastic Finite Element Method," *Computational Mechanics*, **71**: 917–933. https://doi.org/10.1007/s00466-022-02259-7

Shinozuka M and Sato Y (1967), "Simulation of Nonstationary Random Process," *Journal of the Engineering Mechanics Division*, **93**(1): 11–40. https://doi.org/10.1061/JMCEA3.0000822

Sun LM, Xie WP, He XW and Hayashikawa T (2016), "Prediction and Mitigation Analysis of Ground Vibration Caused by Running High-Speed Trains on Rigid-Frame Viaducts," *Earthquake Engineering and Engineering Vibration*, **15**(1): 31–47. https://doi.org/10.1007/s11803-016-0303-7

Tan JC, Xiang P, Zhao H, Yu J, Ye BL and Yang DL (2022), "Stochastic Analysis of Train Running Safety on Bridge with Earthquake-Induced Irregularity under Aftershock," *Symmetry*, **14**(10): 1998. https://doi.org/10.3390/sym14101998

Wang XW, Li ZQ and Shafieezadeh A (2021a), "Seismic Response Prediction and Variable Importance Analysis of Extended Pile-Shaft-Supported Bridges Against Lateral Spreading: Exploring Optimized Machine Learning Models," *Engineering Structures*, **236**: 112142. https://doi.org/10.1016/j.engstruct.2021.112142

Wang YW, Li XJ, Wang ZF, Shi JP and Bao EH (2021b), "Deep Learning for P-Wave Arrival Picking in Earthquake Early Warning," *Earthquake Engineering and Engineering Vibration*, **20**(2): 391–402. https://doi.org/10.1007/s11803-021-2027-6

Xia H, Zhang N and Guo WW (2018), *Dynamic Interaction of Train-Bridge Systems in High-Speed Railways*: *Theory and Application*, Beijing Jiaotong University Press (China) and Springer (Germany). https://doi.org/10.1007/978-3-662-54871-4

Xia XS, Wu SW, Shi J, Jia JF, Chen XC and Ma HJ (2020), "Seismic Response of Rocking Isolated Railway Bridge Piers with Sacrificial Components," *Earthquake Engineering and Engineering Vibration*, **19**(4): 1005–1015. https://doi.org/10.1007/s11803-020-0610-x

Xiang P, Ma HK, Zhao H, Jiang LZ, Xu SP and Liu X (2023a), "Safety Analysis of Train-Track-Bridge Coupled Braking System Under Earthquake," *Structures*, **53**: 1519–1529. https://doi.org/10.1016/j.istruc.2023.04.086

Xiang P, Zhang P, Zhao H, Shao ZJ and Jiang LZ (2023b), "Seismic Response Prediction of a Train-Bridge Coupled System Based on a LSTM Neural Network," *Mechanics Based Design of Structures and Machines*, **2023**: 2260469. https://doi.org/10.1080/15397734.2023.2260469

Xu L, Li Z, Zhao YS, Yu ZW and Wang K (2020), "Modelling of Vehicle-Track Related Dynamics: A Development of Multi-Finite-Element Coupling Method and Multi-Time-Step Solution Method," *Vehicle System Dynamics*, **60**(4): 1097–1124. https://doi.org/10.1080/00423114.2020.1847298

Xu L and Lu T (2021), "Influence of the Finite Element Type of the Sleeper on Vehicle-Track Interaction: A Numerical Study," *Vehicle System Dynamics*, **59**(10): 1533–1556. https://doi.org/10.1080/00423114.2020.1769847

Xu L and Zhai WM (2017), "Stochastic Analysis Model for Vehicle-Track Coupled Systems Subject to Earthquakes and Track Random Irregularities," *Journal of Sound and Vibration*, **407**: 209–225. https://doi.org/10.1016/j.jsv.2017.06.030

Xu WJ and Gao MT (2012), "Calculation of Upper Limit Earthquake Magnitude for Northeast Seismic Region of China Based on Truncated G-R Model," *Chinese Journal of Geophysics*, **55**(5): 1710–1717. https://doi.org/10.6038/j.issn.0001-5733.2012.05.027

Zeng ZP, He XF, Zhao YG, Yu ZW, Chen LK, Xu WT and Lou P (2015a), "Random Vibration Analysis of Train-Slab Track-Bridge Coupling System Under Earthquakes," *Structural Engineering and Mechanics*, **54**(5): 1017–1044. https://doi.org/10.12989/sem.2015.54.5.1017

Zeng ZP, Zhao YG, Xu WT, Yu ZW, Chen LK and Lou P (2015b), "Random Vibration Analysis of Train-Bridge Under Track Irregularities and Traveling Seismic Waves Using Train-Slab Track-Bridge Interaction Model," *Journal of Sound and Vibration*, **342**: 22–43. https://doi.org/10.1016/j.jsv.2015.01.004

Zhai WM (2020), *Vehicle–Track Coupled Dynamics: Theory and Applications*, Springer Press (China) and Springer (Germany). https://doi.org/10.1007/978-981-32-9283-3

Zhai WM, Han ZL, Chen ZW, Ling L and Zhu SY (2019), "Train–Track–Bridge Dynamic Interaction: a State-of-the-Art Review," *Vehicle System Dynamics*, **57**(7): 984–1027. https://doi.org/10.1080/00423114.2019.1605085

Zhang XY, Lu ZH and Zhao YG (2023), "The GCO Method for Time-Dependent Structural Reliability Assessment," *Journal of Engineering Mechanics*, **149**(1): 0002178. https://doi.org/10.1061/(ASCE)em.1943-7889.0002178

Zhang ZC, Zhang YH, Lin JH, Zhao Y, Howson WP and Williams FW (2011), "Random Vibration of a Train Traversing a Bridge Subjected to Traveling Seismic Waves," *Engineering Structures*, **33**(12): 3546–3558. https://doi.org/10.1016/j.engstruct.2011.07.018

Zhao H, Wei B, Guo PD, Tan JC, Xiang P, Jiang LZ, Fu WC and Liu X (2023a), "Random Analysis of Train-Bridge Coupled System Under Non-Uniform Ground Motion," *Advances in Structural Engineering*, **26**(10): 1847–1865. https://doi.org/10.1177/13694332231175230

Zhao H, Wei B, Jiang LZ and Xiang P (2022), "Seismic Running Safety Assessment for Stochastic Vibration of Train–Bridge Coupled System," *Archives of Civil and Mechanical Engineering*, **22**(4): 180(2022). https://doi.org/10.1007/s43452-022-00451-3

Zhao H, Wei B, Jiang LZ, Xiang P, Zhang XB, Ma HK, Xu SP, Wang L, Wu H and Xie XN (2023b), "A Velocity-Related Running Safety Assessment Index in Seismic Design for Railway Bridge," *Mechanical Systems and Signal Processing*, **198**: 110305. https://doi.org/10.1016/j.ymssp.2023.110305

Zhao H, Wei B, Shao ZJ, Xie XN, Jiang LZ and Xiang P (2023c), "Assessment of Train Running Safety on Railway Bridges Based on Velocity-Related Indices Under Random Near-Fault Ground Motions," *Structures*, **57**: 105244. https://doi.org/10.1016/j.istruc.2023.105244

Zhao YG and Lu ZH (2008), "Cubic Normal Distribution and Its Significance in Structural Reliability," *Structural Engineering and Mechanics*, **28**(3): 263–280. https://doi.org/10.12989/sem.2008.28.3.263

Zhao YG and Lu ZH (2021), *Structural Reliability: Approaches from Perspectives of Statistical Moments*, Wiley-BlackWell, USA.

Zhao YG and Ono T (2000), "New Point Estimates for Probability Moments," *Journal of Engineering Mechanics-ASCE*, **126**(4): 433–436. https://doi.org/10.1061/(ASCE)0733-9399(2000)126:4(433)

Zhao YG, Weng YY and Lu ZH (2021), "An Orthogonal Normal Transformation of Correlated Non-Normal Random Variables for Structural Reliability," *Probabilistic Engineering Mechanics*, **64**: 103130. https://doi.org/10.1016/j.probengmech.2021.103130

Appendix

Table A1 Parameters of the tractor and trailer (partial data refer to Jiang *et al*. (2019))

Notation	Unit	Tractor/Trailer	Notation	Unit	Tractor/Trailer
m_c	kg	$4.8\times10^4/4.4\times10^4$	k_{2x}	N/m	$0.24\times10^6/0.28\times10^6$
m_t	kg	$3.2\times10^3/2.4\times10^3$	k_{2y}	N/m	$0.4\times10^6/0.3\times10^6$
m_w	kg	$2.4\times10^4/2.4\times10^4$	k_{2z}	N/m	$0.48\times10^6/0.56\times10^6$
W_{axle}	kg	$1.60\times10^4/1.46\times10^4$	c_{1x}	N/(m/s)	$5.0\times10^4/0$
f_{c1}	Hz	0.78/0.84	c_{1y}	N/(m/s)	$5.0\times10^4/5.0\times10^4$
f_{c2}	Hz	1.09/1.06	c_{1z}	N/(m/s)	$3.0\times10^4/3.0\times10^4$
k_{1x}	N/m	$9.0\times10^6/1.5\times10^7$	c_{2x}	N/(m/s)	$6.0\times10^4/12\times10^4$
k_{1y}	N/m	$1.04\times10^6/0.7\times10^6$	c_{2y}	N/(m/s)	$6.0\times10^4/6.0\times10^4$
k_{1z}	N/m	$3.0\times10^6/5.0\times10^6$	c_{2z}	N/(m/s)	$3.0\times10^4/2.5\times10^4$

Table A2 Parameters of the track slabs and bridge (partial data refer to Liu *et al*. (2020b) and Zeng *et al.* (2015))

Notation	Definition	Unit	Value
	Track slab		
$\overline{m}_r$	Mass per unit length of the rail	kg/m	60.64
I_{ry}	Flexural moment of inertia about the *y*-axis of a cross-section of the rail	m^4	3.22×10^{-5}
I_{rz}	Flexural moment of inertia about the *z*-axis of a cross-section of the rail	m^4	5.24×10^{-6}
$\overline{m}_s$	Mass per unit length of the slab	kg/m	1.2×10^3
I_{rz}	Flexural moment of inertia about the *y*-axis of a cross-section of slab	m^4	1.4×10^{-3}
I_{sz}	Flexural moment of inertia about the *z*-axis of a cross-section of slab	m^4	0.22
k_{rsy}	Lateral stiffness of a fastener	N/m	3.0×10^7
k_{rsz}	Vertical stiffness of a fastener	N/m	5.0×10^7
	Bridge		
E_b	Elastic modulus	N/m^2	3.45×10^{10}
I_b	Mass moment of inertia of a cross-section	m^4	12.744
μ	Poisson's ratio	–	0.2
$\overline{m}_b$	Mass per unit length	kg/m	2.972×10^4
L_e	Length of the element	m	3.2
ζ	Damping ratio	–	0.05